Available online at www.sciencedirect.com

SciVerse ScienceDirect

Ceramics International 39 (2013) 183–195

CERAMICS INTERNATIONAL

www.elsevier.com/locate/ceramint

Hydroxyapatite-doped poly(lactic acid) porous film coating for enhanced bioactivity and corrosion behavior of AZ31 Mg alloy for orthopedic applications

Abdalla Abdal-hay[a,b], Nasser A.M. Barakat[c,d], Jae Kyoo Lim[b,*]

[a]Department of Bionano System Engineering, College of Engineering, Chonbuk National University, Jeonju 561-756, Republic of Korea
[b]Department of Mechanical Design Engineering, Advanced Wind Power System Research Institute, Chonbuk National University, Jeonju 561-756, Republic of Korea
[c]Organic Materials and Fiber Engineering Department, Chonbuk National University, Jeonju 561-756, Republic of Korea
[d]Chemical Engineering Department, Minia University, El-Minia, Egypt

Received 27 April 2012; received in revised form 5 June 2012; accepted 5 June 2012
Available online 13 June 2012

Abstract

The corrosion behavior of magnesium and its alloys in the electrolytic physiological environment is extremely poor; this imposes a limitation for their use in orthopedic applications. In the present study, the effect of spray coating AZ31 magnesium alloy with membrane films of pristine and hydroxyapatite-doped poly(lactic acid) on corrosion behavior and bioactivity is investigated. Polymer concentration was found to have a strong impact on the pore size of the coating layer. However, addition of HAp NPs distinctly stimulated the precipitation of an apatite-like compound upon soaking the samples in a simulated body fluid (SBF). Magnesium coated samples revealed three orders of magnitude less corrosion compared to the naked samples, which indicates a stable electrochemical corrosion resistance. During a 15 days *in-vitro* test, pH variation, weight loss, and bending strength were lower for the coated samples (with average values of 8.5%, 7.2% and 10%, respectively) than the control sample (10.5%, 15.5%, and 25%, respectively). Moreover, the coated samples showed good bending strength characteristics. Cytocompatibility studies on MC3T3 cells revealed a continuous increase in cell growth with the coated samples. Overall, the suggested strategy might open a new avenue to widen utilization of Mg alloys as implant materials for orthopedic applications.

Keywords: Mg alloys; Poly (lactic acid); Orthopedic applications; Biodegradable implants

1. Introduction

The global accident rates involving bone fractures increase gradually every year. A considerable percentage of these fractures are too complex to simply medicate externally and thus have to be fixed using surgical bone implants. Commonly used materials for fixing bone fracture are medical-grade metals such as 316L stainless steel, pure titanium and its alloys, and cobalt–chromium-based alloys [1]. If the implant carries too large a component of the applied load, the bone beneath it will experience a reduced load and will lose density in response [2]. The properties of these conventional metallic implants do not match well with bone due to the basic difference in the modulus of elasticity of the two (for cortical bone, in the order of 3–20 GPa, which is an order of magnitude less than that of metals [1,3,4]). In case of metal implants, risk of stress shielding of the bone is much higher since a greater portion of the load is on the metallic implants. This stress shielding obstructs the stabilization of the bone tissue and hence multiple surgeries need to be performed, leading to further complications. Magnesium alloys, in contrast, have a modulus of elasticity of around 45 GPa, which is much closer to that of bone, which could thus lessen the likelihood of stress shielding and associated loss of bone density.

Biodegradability of the magnesium alloys is another preferable advantage compared with conventional

*Corresponding author. Tel.: +82 63 270 2321; fax: +82 63 270 4439.
E-mail address: jklim@jbnu.ac.kr (J.K. Lim).

0272-8842/$36.00
http://dx.doi.org/10.1016/j.ceramint.2012.06.008

implants, which are well-known non-degradable materials. An implant's ability to degrade after the bone heals is a much-desired characteristic. Long-term adverse effects or even an increased risk of local inflammation may occur after long-term implantation since the metallic implant is a foreign body to human tissues [5]. If this is the case, a second surgery is conducted for implant removal. However, repeated surgery not only increases the morbidity rate of patients, but also results in an increase of health care costs and longer hospitalization [1].

At the first half of the last century, feasibility studies showed high biocompatibility and good restorability level of magnesium bone-fixation implants [6]. However, one cannot ignore the undesirably high degradation rate of magnesium and its alloys, which is a major concern for using it as an implant material. The high corrosion/degradation rates cause the formation of unwanted, possibly harmful hydrogen gas pockets under the skin that cause failure of a surgery before the healing process can occur, and may also be deleterious to the surrounding tissues [7]. Gas evolution can be avoided by controlling the degradation rate of the magnesium alloys. The enhancement of the corrosion resistance of magnesium can be achieved by using different modification methods such as alloying [8,9] and various surface treatments [10]. Some authors [8,9,11] have suggested that magnesium alloys, especially those containing rare earth elements, seem to be suitable for use as orthopedic implants. However, in addition to the alteration of its original mechanical properties, the addition of rare earth metals such as zirconium and cerium into the magnesium substrate may potentially add toxic effects to cells [8,9], as the cytocompatibility of these elements is not well known. Recently, researchers have suggested coating the metal as an effective and safe strategy to regulate the degradation rate of Mg and its alloys. For instance, Wong et al. [12] were able to reduce the release of magnesium ions by depositing poly-ε-caprolactone (PCL) polymer membranes on Magnesium alloy (AZ91) at two different solution concentrations, which could control the degradation rate of AZ91 alloy in *in-vitro* and *in-vivo* environments. However, pristine polymer does not seem to be a good coating material as it does not stimulate precipitation of apatite-like compounds [13]. To use coated-Mg in orthopedic applications, the coating must be non-toxic, bioactive, and control its degradation rate to a moderate value.

Hydroxyapatite (HAp, $Ca_{10}(PO_4)_6(OH)_2$) is used for bone tissue engineering due to its excellent biocompatibility, bioactivity (chemical bonding ability with natural bone), slow in situ biodegradability, high osteoconductive and/or osteoinductive non-toxicity, non-inflammatory behavior, and non-immunogenicity properties with soft tissue and hard tissue [14–18]. Therefore, HAp can be a suitable material for coating Mg/Mg-alloy after proper investigations.

In this study, HAp-doped poly(lactic acid) membrane is studied as a coating layer on AZ31B magnesium alloy to simultaneously control the degradation rate and activate bone formation. The utilized physiochemical characterizations strongly support the suitability of the proposed coating layer for the Mg alloys, as observed during *in-vitro* studies.

2. Materials and process

2.1. Materials

The following chemicals were used without further purification or modification: calcium nitrate tetrahydrate ($Ca(NO_3)_2 \cdot 4H_2O$), diammonium hydrogen phosphate ($(NH_4)_2HPO_4$) (Showa Chemical, Japan), aqueous ammonia solution, ethanol (Samchun pure chemical, South Korea), dichloromethane (DCM) (Junse Chemical, Japan), and polylactide (PLA) with an average molecular weight (Mw) of 160,000 (Showa Chemical, Japan). Hank's balanced salt solution was supplied from Sigma Aldrich and was utilized as a simulated body fluid (SBF).

2.2. Synthesis of HAp nanopowder

HAp nanopowder was synthesized using a wet chemical procedure. 0.6 M $(NH_4)_2HPO_4$ aqueous solution was added at a rate of 0.4 ml min^{-1} to 1 M $Ca(NO_3)_2 \cdot 4H_2O$ aqueous solution under strong stirring (The Ca/P ratio was 1.67 when these solutions are mixed to produce stoichiometric HAp); ammonium solution was used to adjust the pH of the solution to 11. After stirring the solution at room temperature (RT) for 3 h, it was heated to 90 °C for 1.5 h under continuous stirring. The resultant precipitate was kept for 24 h at RT under vigorous stirring to produce a homogeneous solution. Finally, the milky solution was filtered, and the precipitate was washed several times by a mixture of distilled water and alcohol (volume ratio = 1:1) until pH was neutralized (i.e. 7). The final precipitated HAp was dispersed in alcohol to modify the agglomeration of the obtained powder. The synthesized powder was dried in vacuum for 24 h and then calcined at 650 °C for 4 h in ambient air with a heating rate of 20 °C min^{-1}.

2.3. Sample preparation and surface treatment

Die-cast magnesium alloy AZ31B (2.47% Al, 0.63% Zn, bal Mg (wt%)) was chosen as the substrate material and as a control. AZ31B was not commercially purchased but instead prepared using high purity magnesium 99.99% by colleagues and is reported elsewhere [8]. AZ31B alloy was cut into disc specimens 12 mm in diameter (cross section area around 1 cm^2) and 2 mm in thickness for *in-vitro* degradation and cytotoxicity experiments. Before coating, the samples were pre-treated as follows: (1) first, they were grinded and polished mechanically with silicon carbide papers (800–1500 grits) and soft cloths to ensure the same surface roughness, then they were (2) cleaned ultrasonically in acetone for 5 min

to remove residual grease and distilled water and dried in a normal dryer at 45 °C.

2.4. Coating procedure

The deposited membrane layers were prepared according to the following process: two PLA solutions (3.22 and 4.75 wt/v) were prepared by dissolving polymer granules in dichloromethane (DCM) solvent. Colloids were prepared by mixing the synthesized HAp nanoparticles with the obtained PLA solutions and stirred continuously for more than 24 h. Four colloids were prepared using two concentrations of HAp (1 and 1.5 wt%) with every PLA solution. In total, six different formulations (2 pristine PLA solutions and 4 colloids) were prepared and investigated as coating layers on Mg-alloy substrate. These solutions were coated using a custom designed spraying device [12] at room temperature and 50% humidity. The air pressure (400 kPa) was optimized for fine droplets. The coated samples were dried in a vacuum oven for 12 h at 40 °C (less than T_G of the PLA; T_G=53 °C). Further, to improve adhesion on the substrate samples, surfaces were heated to 67 °C for 1.5 h.

2.5. In-vitro degradation test

Hank's solution was used as a standard simulation body fluid (SBF) for immersion testing. Four specimens for each type were immersed in 50 ml of the solution with a surface area to solution volume ratio of 1 cm^2:20 ml. The solution temperature was maintained at 37 ± 0.2 °C during the test. The samples were soaked for different time intervals, after which they were gently rinsed with flow-distilled water and then dried at room temperature. Then surface morphology was examined using scanning electron microscopy (SEM) equipped with an energy dispersive spectrometer (EDS). The pH values of the coated and control samples were recorded at different times. The degradation rate of the Mg substrate was determined by measuring the relative percentage weight loss of the samples according to the relation:

$$M_L = \left(\frac{M_t - M_0}{M_0}\right) \times 100, \quad (1)$$

where M_L, M_0, and M_t are the percentage weight loss, and the weights before and after immersion, respectively. Prior to weight loss analysis, all the samples were immersed in chromic acid [19] for five minutes to remove the hydroxide layer formation from the surface of the samples.

2.6. Electrochemical corrosion test

The electrochemical behaviors of both the control and coated samples were investigated using a potentiodynamic polarization test (263A, EG&G PAR, USA). Prior to polarization test, the samples were immersed in 1000 ml SBF for 20 min. A three-electrode cell was constructed to perform the test with the samples used as the working electrode, saturated potassium chloride electrode as the reference electrode, and platinum as the counter electrode. The exposed area of the working electrode (control and deposited samples) to the solution was 0.785 cm^2. A scanning rate of 1 mVs^{-1} was applied during the test, which started at −160 mV. The changes in the free corrosion potential were recorded as a function of time. The temperature was controlled at 37 ± 0.5 °C. The corrosion rates of the samples were calculated by extrapolating the polarization curve according to ASTM-G102-89 [20].

2.7. Mechanical properties test

The bending strength was determined as the maximum point of the stress–displacement curve using a three point bending test, which was conducted in a standard laboratory atmosphere with a mechanical tester (Computerized Instron Universal Testing Instrument model 4206). The test samples were conducted at an across-head speed of 0.5 mm/min and with a span length of 25 mm. The samples were prepared with dimensions of 33 × 5 × 5 mm, which is required for testing. At least four specimens were tested for each sample.

2.8. Determination of cytotoxicity and cell viability assay

Cytotoxicity assessments were carried out using MC3T3 cells which were cultured in Dulbecco's modified Eagle's medium (DMEM) (Gibco Co,USA), supplemented with 10% fetal bovine serum (FBS) in a humidified incubator with 5% CO_2 and 95% relative humidity at 37 °C. The extraction media were at 100% concentration after one-day incubation in a humidified atmosphere with 5% CO_2 at 37 °C. The test was established by using an indirect method, where the immersion extracts collected from the immersion test were used for culturing cells. The DMEM medium acted as a negative control while DMEM medium containing 20% dimethyl sulfoxide (DMSO, Sigma) was used as a positive control. Cells were incubated in 24-well flat-bottomed cell culture plates at 5×10^4 cells/ml in each well, and incubated for one day to allow cell attachment. Then, the medium was replaced by 1 ml of extraction medium. After incubation in a humid atmosphere for 1, 2 and 3 days, cells were fixed in PBS containing 3% formaldehyde and 0.2% glutaraldehyde and then stained with 0.3% crystalviolet. Cell morphology was observed by stereoscopic microscopy (Leica microsystem DE/EX 4, Germany). 5 mg per ml stock solution of MTT dye (3-[4,5-dimethylthiazol-2-yl]-2, 5-diphenyl tetrazolium bromide, Sigma) was made in sterile phosphated buffered saline (PBS). 200 μm MTT was then added to each well and the untreated and treated samples were incubated for 4 h (5% CO_2 and 95% relative humidity at 37 °C). Following that, 1 ml dimethyl sulfoxide (DMSO, Sigma Aldrich) was added to each well and optical density (OD) was measured at 540 nm using ELISA (Benchmark

microplate reader, BIO-RAD, California, USA). The percentage of RGR values (OD for coated specimen/OD for negative control group × 100%) were calculated and drawn as a function of time/day. A larger RGR value represents higher cell viability and thus adhesion. Statistical significance was defined as $P < 0.05$.

2.9. General characterization

Scanning electron microscopy (SEM) images were obtained by a scanning electronic microscope (JEOL JSM 820, USA) coupled with an energy dispersive spectrometer (EDS) detector. The internal characterization was investigated using *transmission electron microscopy* (*TEM*, CM 200, Philips) with an accelerating voltage of 200 kV. The phase composition was characterized by an *X-ray diffractometer* (*XRD*, Rigaku, X'Pert X-ray diffractometer, using Cu Kα target, 2θ in the range of 10–70°). The thickness of the deposit layer for the coated samples was measured by Alpha step method (KLA-TENCOR Alpha Step IQ) according to the next step, and a coating piece close to the sample edges was removed using a sharp blade, and the gap between the coated and uncoated area was identified. The viscosity was measured by a Brookfield, DV-III ultra programmable Rheometer at room temperature. The wettabilities of the coated samples were investigated with deionized water, and contact angle measurements were made using a contact angle meter (GBX, Digidrop, France). Deionized water was automatically dropped (drop diameter 6 μm) onto the sample. The measurement was carried out after 5 s after the water droplet. The measurements were carried out at room temperature. The utilized thin films have been coded according to the concentration of PLA solution. Typically, as the lower concentration (3.22 wt/v) PLA solution/colloids revealed high porosity surface compared with the higher concentration (4.76 wt/v) solutions, they are coded as HPMx (high porous membrane, x points to the HAp content), while the other formulations were named as LPMx (low porous membrane). Table 1 summarizes the rheological properties of the utilized formulations as well as the solvent used.

3. Results and discussion

3.1. Synthesis and characterization of the HAp nanoparticles

In this study, the synthesis of nanocrystal HAp powders was carried out via wet chemical precipitation without any aid of surfactants or co-surfactants since they do not have adequate biological properties and are suspected to produce allergic reactions due to their non-biodegradability [21]. The size and morphology of the as-synthesized HAp and the calcined samples were examined using TEM images. As shown in Fig. 1(a) and (c), the dried precipitate shows needle-like structure with relatively large size, having a dimension range 15–20 nm in width and 120 ± 20 nm in length; and an aspect ratio ranging from 2 to 8. In contrast, nanoparticles (with few needle-like HAp formations) (Fig. 1b and d) were obtained due to calcination of the dried powder at a temperature of 650 °C. This result is consistent with other reference reports [22,23]. There could be two reasons for HAp nano-needle like structures changing into nanoparticles upon calcination. The first reason is that HAp is a brittle material that can break into pieces when heated to a high calcination temperature. The second reason may be due to excess residual solvent (H_2O) in the as-dried HAp. As shown in Fig. 1(b), which represents the calcined sample, the nanoparticles have an average diameter of 120 ± 30 nm. It can be seen in HRTEM images (Fig. 1d) that the calcined HAp has higher crystallinity than the dried sample (Fig. 1c). Moreover, less agglomeration and more uniform distribution features can be observed in the caclined sample. The spherical geometry is responsible for achieving osseointegration. [22] Therefore, the calcined powder is preferred for biomedical coating applications [21].

Fig. 2 shows the XRD patterns of the synthesized and calcined HAp powder. As shown in the figure, the spectrum corresponding to the dried sample has low and travail peaks denoting HAp, which indicates low crystalinity and/or small and disordered grains. Moreover, a considerable shift can be observed. However, for the calcination process that led to the high and sharp peaks shown in the spectrum of the sintered powder, all the peaks allocate at standard diffraction angles. This indicates that the calcination process enhances the obtained powder

Table 1
Sample code, viscosity of the utilized solution in the coating process, and water contact angle of the obtained coats.

	Sample	Sample code	Viscosity (cP)	Water contact angle (deg.)
DCM	–	–	0.39	–
LPM	4.76 PLA + 0%HAp	LPM1	28.8	54 ± 0.5
	4.76 PLA + 1%Hap	LPM2	88.8	58 ± 0.5
	4.76 PLA + 1.5%Hap	LPM3	93.6	67.6 ± 0.5
HPM	3.22 PLA + 0%Hap	HPM1	12.5	–
	3.22 PLA + 1%HAp	HPM2	–	–
	3.22 PLA + 1.5%HAp	HPM3	–	–

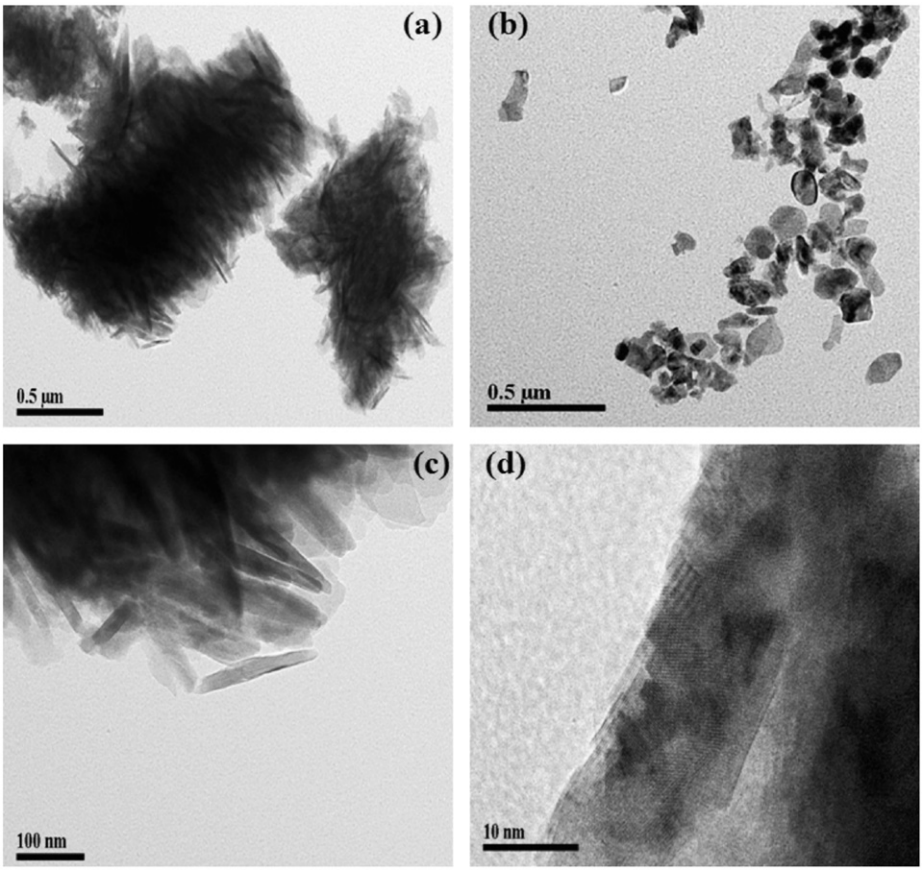

Fig. 1. TEM images of the synthesized HAp; (a) and (c) represent the dried samples, while (b) and (d) show the calcined samples at 650 °C.

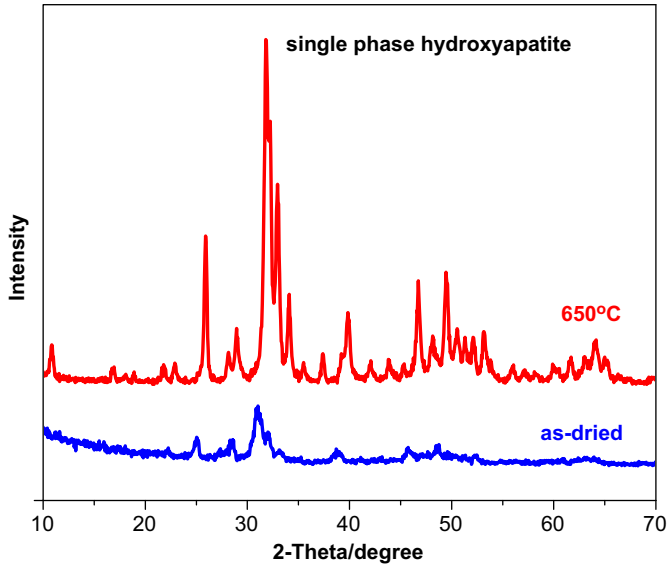

Fig. 2. X-ray diffraction patterns for the dried and sintered HAp powders.

crystalinity. Other impurities such as CaO and b-tri-calcium phosphate could not be detected [24] (within the detection limit of XRD), which indicates pureness of the synthesized powder. The observed spectrum well matches the standard JCDPS file # 09-0432 (HAp).

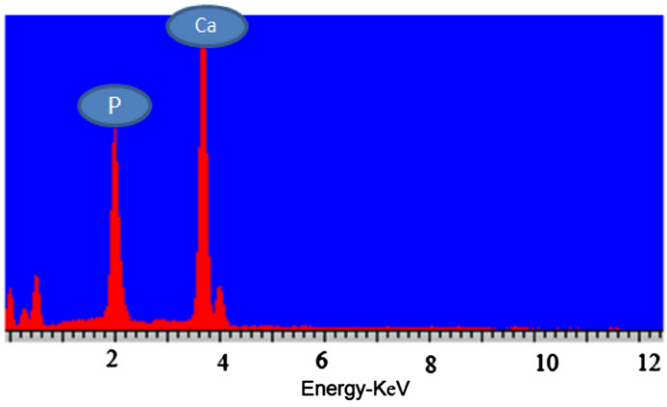

Fig. 3. EDS results of synthesized HAp NPs.

To further confirm the XRD observations, elemental analysis of calcined HAp powder was also carried out using EDS, and the corresponding spectrum is shown in Fig. 3, where only peaks related to Ca and P could be observed. These results confirm that the surfactants-free precipitation method is an effective route to prepare the nanorods and/or nanoparticles of crystalline and single-crystal HAp, and the calcination temperature has an influence on its morphology.

3.2. Characterization of the coating layers

3.2.1. Surface morphology and porous properties

Generally, the coating layers mainly contain three different layers: the primer, intermediate and top-coating layers. The first is responsible for enhancing the adhesion of the other layers to the substrate surface as well as for corrosion protection. The intermediate layer is responsible for determining the final coating thickness, and the top-coating layer produces the desired surface properties. More detailed information on the three layer formations can be found in the literature [25–27].

Fig. 4(a)–(f) show SEM images of the pristine and doped PLA membranes. Highly ordered porous films obtained

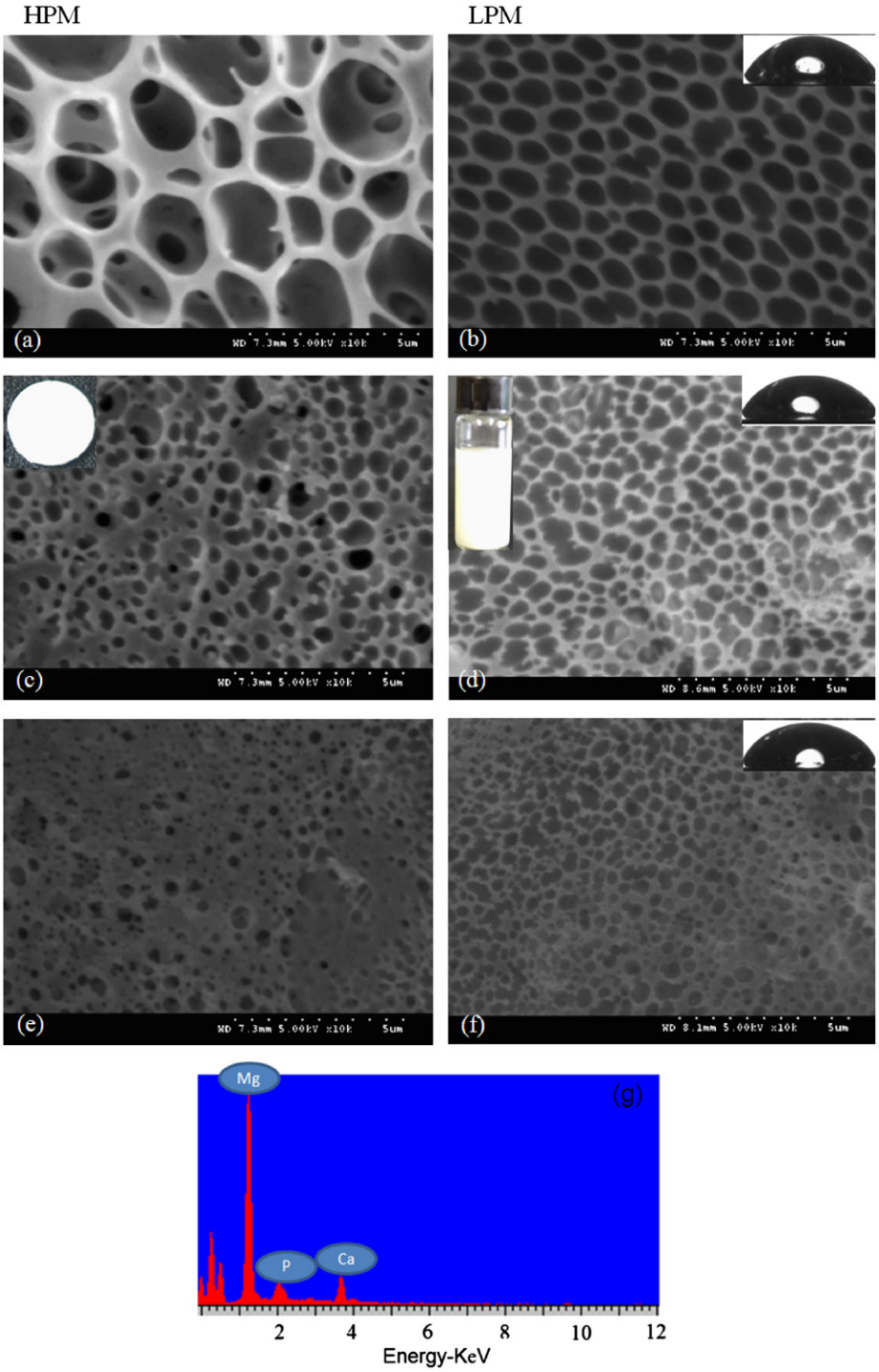

Fig. 4. Surface SEM images of pure PLA and PLA/HAp composite membranes; (a) HPM1, (b) LPM1(the inset shows a photo for the coated disk), (c) HPM2, (d) LPM2 (Hanging solution for the composite sample, inset), (e) HPM3, (f) LPM3 (g) EDS of the composite membranes.(b, d, and f, the insets represent the corresponding water contact angles at 5 s).

with all formulations can be seen in these SEM images. It can be also seen that incorporation of HAp NPs did not affect the porosity of the coated layer, probably due to the small size of the utilized NPs compared to the pore diameters, as they might be embedding inside these pores.

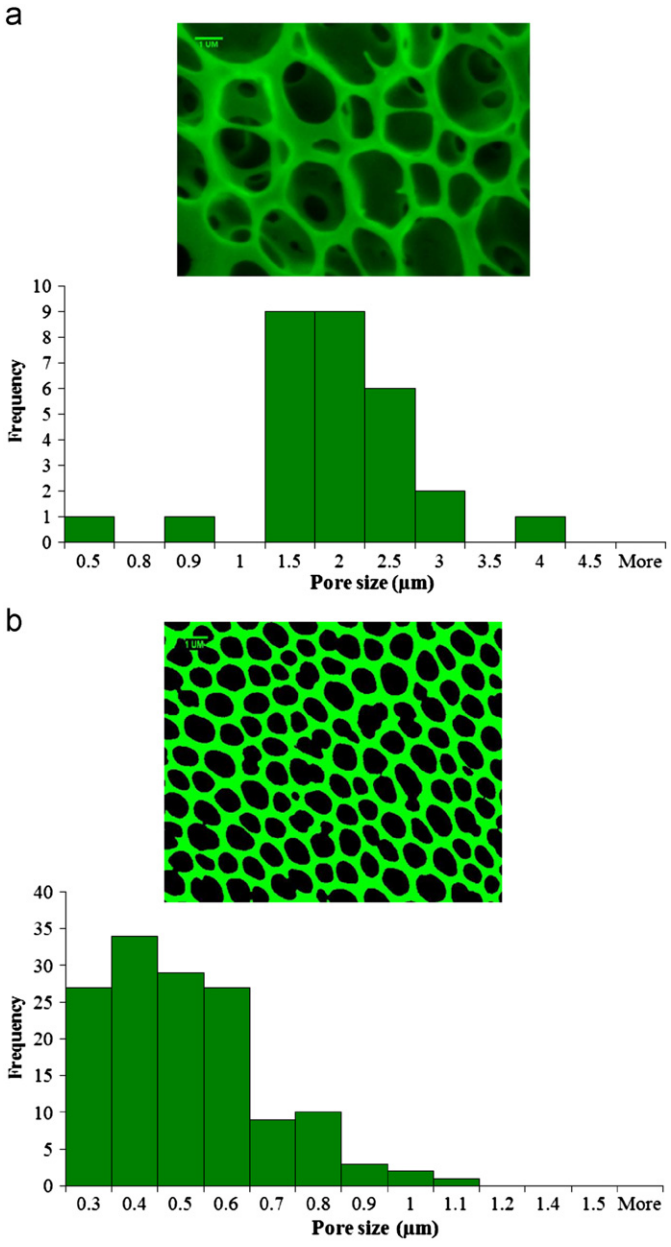

Fig. 5. Characterization of the pores structure by using ImageJ analysis (a) HPM1 and (b) LPM1.

One can also conclude that increasing the polymer concentration leads to decreased porosity in the obtained coating layer. The inset shows the respective water contact angles.

The SEM images were processed using ImageJ software to estimate the pore size and distribution. Results of the image processing for HMP1 and LMP1 formulations are shown in Fig. 5(a) and (b), respectively, and values are listed in Table2. A similar trend is observed for other formulations thus data are not presented. The porosity changed from ca. 71% to ca. 58% for these two formulations with an average pore size of ~1.8 and 0.76 μm, respectively. It is believed that such highly porous films could be obtained because of solvent evaporation. Liu et al. [28] reported that the morphology of PLA membranes is strongly influenced by the solvent concentration. When the weight content of PLA was less than 15 wt%, a porous structure was formed by a liquid–liquid de-mixing process. Consistent with that study, as shown in Fig. 5 and Table 2, low concentration PLA solution (i.e. in HPM1 sample) produced pore size in the range of 0.414 to 3.818 μm (average value 1.789 μm), and the pore area was 77 μm^2 (porosity is 70.9%). However, the average pore size decreased to 0.764 μm in the LPM1 sample, and the corresponding porosity was 58% (Table 2). It is reported that the pore size significantly depends on the concentration of the polymer solution, since concentrated polymer solution produces smaller pores due to the existence of less polymer-poor phase [12,29]. The pore size becomes smaller by the addition of HAp content; i.e. the microporous gets interconnected because these particles fill the membrane (as seen in Fig. 4c–f). Fig. 4(g) presents the EDS spectrum of the composite membrane formulation, which clearly shows the presence of HAp (i.e. Ca and P) inside the pores, even though SEM could not visualize it.

3.2.2. Water contact angle

It is known that the microstructure and chemical structure of the material's surface play a key role in the *in-vitro* bioactivity in aqueous environments. Therefore, surface properties such as surface free energy and wettability are critical to the biological performance of materials [30]. The insets of Fig. 4(b), (d) and (f) are the water contact angles at five seconds for LPM1, LPM2, and LPM3 membrane layers, respectively. The contact angle values of the different membranes are summarized in Table 1. It is found that pure PLA (LPM1, Fig. 4b) is

Table 2
Characterization of the pristine PLA porous membrane structure.

Sample	Pore length (μm)			Pore area (μm^2)	Total area (μm^2)
	Min	Max	Average		
HPM1	0.414	3.818	1.789	77.03	108.59
LPM1	0.308	1.196	0.764	63.04	108.59

hydrophilic, having low contact angle ca. 54°, which is closer to the reported values in the literature [31], and consequently produces a wetting hysteresis and lower the interfacial free energy. This is because PLA has strong hydrophilicity. Augmented wettability of the PLA layer can help enhance protein adsorption, and hence cell attachment, promoting cell growth, proliferation, and maintaining the differentiated cell phenotype [30]. This is an essential step to ensure that the cells can adhere to the surface of the PLA membranes when deposited on the Mg surface. When the HAp content increased to 1 and 1.5% (LPM2 and LPM3) in the composite membranes, the contact angles also increased slightly (as shown in Fig. 4d and f). The increase in the contact angle may be due to the interconnecting HAp particles in the poor phase of the porous membranes. However, even with HAp embedding, the wetting angles of the utilized layers are still in the acceptable range, so it is expected that all the formulations have hydrophilicity, enhancing the surfaces for biological processes.

3.2.3. Electrochemical corrosion test

Representative potentiodynamic polarization curves obtained from the un-coated and coated AZ31 magnesium samples (LMP1, LMP2 and LMP3) in SBF at 37 °C are presented in Fig. 6. The corrosion potential (E_{Corr}) values are listed as inset in the figure. In general, the E_{Corr} is shifted to the positive side by pristine polymer-coated magnesium alloys. The E_{corr} value of the PLA/HAp composite membranes (LPM2 and LPM3) shifted to positive potential due to the addition of HAp in the membrane layers. At the same time, the values of the corrosion current (I_{corr}) of the doped polymer layers (especially LPM3 sample (1.45×10^{-9} A/cm^{-2})) decreased by three orders of magnitude as to the uncoated sample (4.67×10^{-5} A/cm^{-2}). Such a reduction in corrosion current is correlated to the relative insertion of HAp nanoparticles in pores thereby decreasing the potential surface corrosion area. In addition, hydroxyapatite itself shows high corrosion resistance due to thermal stability. This explains why higher E_{corr} and lower I_{corr} values were observed with the LPM3 compared to the LPM1. In other words, the HAp-doped PLA coating layer could properly perform the desirable task of decreasing the corrosion rate of the Mg alloy compared to the pristine PLA. Therefore, the undesired hydrogen gas evolving due to the corrosion reaction of Mg (Eq. (2)) can be eliminated.

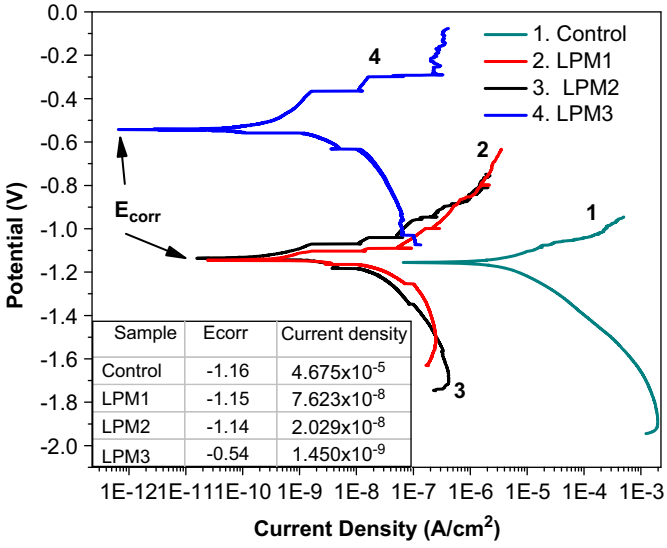

Fig. 6. Potentiodynamic polarization curves of the control sample and samples coated with pristine PLA and PLA/HAp composite membranes.

$$Mg(s) + 2H_2O \rightarrow Mg^{2+} + 2OH^-_{(aq)} + H^{\uparrow}_{2(g)} \text{(overall reaction)} \quad (2)$$

The reported corrosion potential value of AZ31 (−1.67 V in sodium chloride solution [32]) is lower than the value measured in this study, however it is difficult to compare the values since the medium for the corrosion tests are different [33]. It may also be due to the low impurity levels in the alloy used. The reason for selecting SBF in this work is mainly for *in-vitro* analysis.

3.3. Biological activity investigation

3.3.1. Samples surface morphology after immersion in SBF

Fig. 7(a)–(f) typically illustrate the surface morphology and EDS spectra of LPM3 samples and bare Mg substrate after immersion in Hank's solution. It is observed that the bare sample surface (Fig. 7a) contains a number of cracks and sparse precipitate from the bone-like material after one-day immersion time. The EDS (Fig. 7b) reveals that the surface of the bare sample has apatite-like compound (containing Ca and P) deposited on the surface. In contrast, with the same exposure time for LPM3 samples, an enhanced deposition from the bone-like precipitate was observed which is marked by the dashed circles in Fig. 7(c). Moreover, due to the high precipitation rate, some pores were blocked completely and formed into a thin film (the dashed circles in Fig. 7c). The EDS measurement revealed relatively high weight percentages of Ca and P compared to the control sample (Fig. 7d). Additionally, Fig. 7(e) and (f) show the surface morphology after 10 day of immersion for both samples. Even though there are bonelike precipitates on the surface, not all the surface of the bare sample could be covered, which indicates low bioactivity. On the other hand, much higher precipitate could be seen on the surface of the coated materials (Fig. 7f). It is noteworthy that Mg metal lacks desirable bioactive (bone-growth) properties, due to the high degradation rate of Mg and therefore does not motivate attachment on its surface. However, the polymer layer enhances the bioactivity. Moreover, the incorporated HAp nanoparticles at the surface work as nuclei for the newly deposited HAp that enhances the precipitation reaction. Zhou et al. [34] suggested that accelerated precipitation of HAp is beneficial for faster

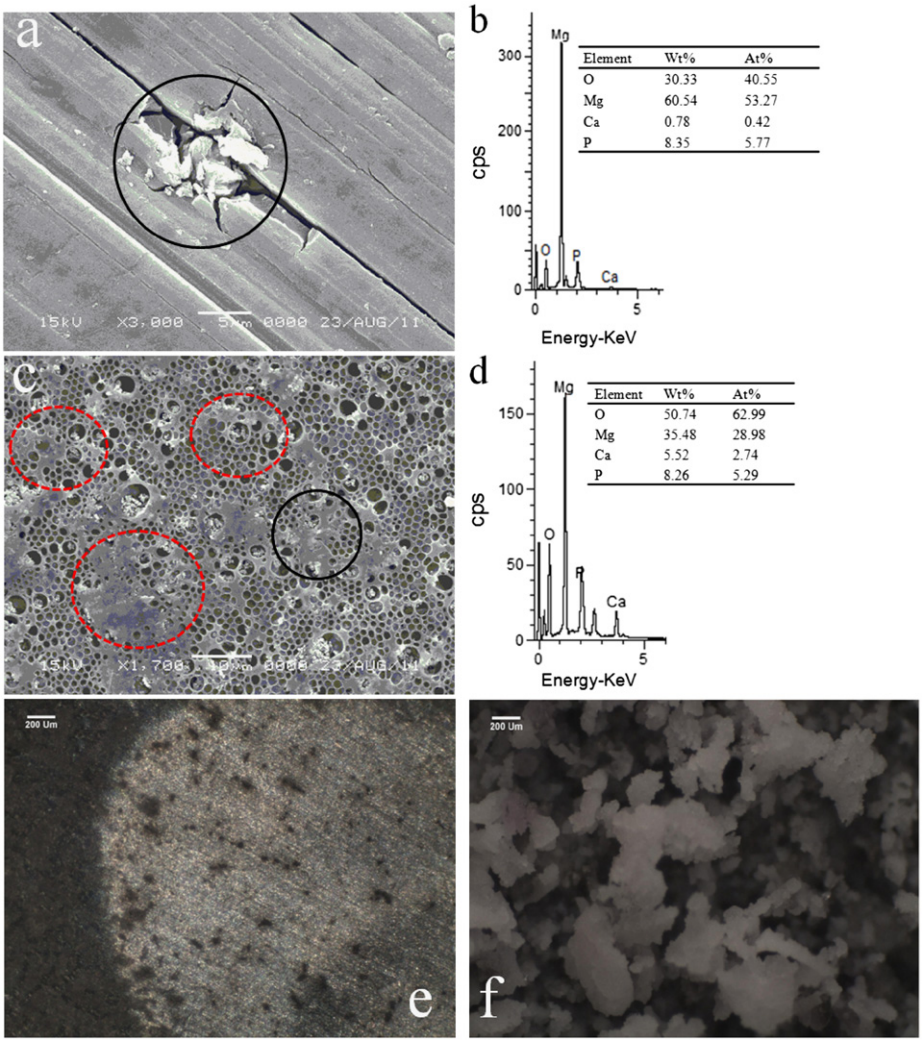

Fig. 7. Surface morphology and EDS spectrum after immersion for1-day (a) bare AZ31 sample, (b) EDS of the marked area in a, (c) AZ31 disk coated with PLA/HAp composite membranes (LPM3) and (d) EDS of the marked area in c, (e) and (f) light optical microscopy of the bare and covered samples with composite membrane (LPM3) after 10 day immersion.

healing of orthopedic patients, as well as for a variety of biomedical diagnostic and therapeutic applications.

3.3.2. *pH variation and degradation rate*

The pH values of the solutions containing the bare and coated samples as a function of time are depicted in Fig. 8. It is found that the pH value of the control and coated samples were found to be between 7.47 to 10.5 and 7.47 to 8.5, respectively, after 15 days of immersion. These results reveal that the pH variation of the coated samples is slower than the control. Moreover, it can be concluded from the figure that an increase in the pH within the first week of immersion of the coated samples is much lower than that of the uncoated. These results are consistent with electrochemical results, as increase in pH value for the control sample indicated high corrosion rates, and vice versa for the coated samples. Fig. 9 shows the degradation rate for coated and uncoated samples in terms of weight loss

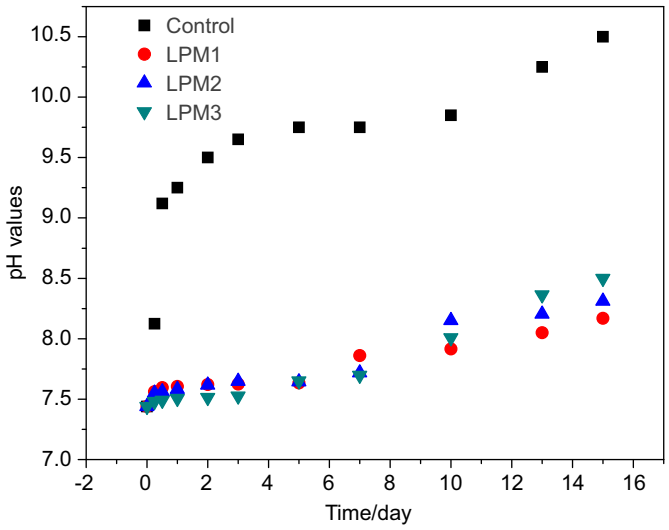

Fig. 8. pH values at different immersion periods in SBF.

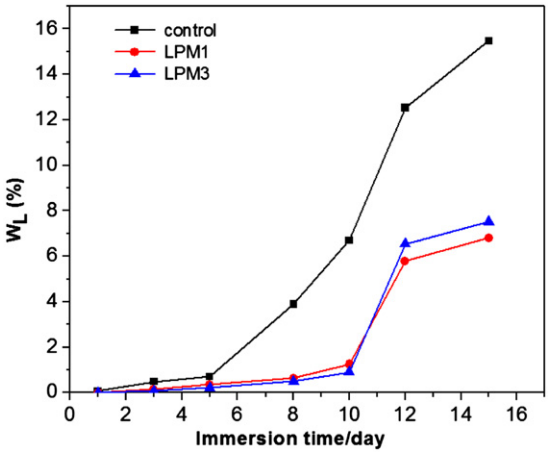

Fig. 9. Total weight losses from the coated and control AZ31 samples over time.

percentages. The total weight loss of the treated samples was lower than that of the control. However, from this figure it can be observed that the degradation rate of the control and coated samples were approximately 15.5% and 7.2% after 15 days of immersion, respectively. The lower degradation rate reveals descending Mg ions released from the surface. It is noteworthy that the literature did not specify a fixed relation between the corrosion rates of the Mg alloys in the *in-vitro* and *in-vivo* conditions. For instance, Witte et al. [11] stated that the corrosion rate in case of the *in-vitro* condition is equal to 4 times the rate in case of *in-vivo*, and other researchers supported this hypothesis [33,35]. On the other hand, other studies [1] reported that the tendency of the degradation in case of the *in-vitro* tests is in the opposite direction as those obtained from the *in vivo* studies. Consequently, *in-vitro* corrosion tests cannot be used to predict the *in-vivo* corrosion rates of magnesium alloys. Therefore, investigations are underway to understand the effect of *in-vivo* study on Mg treated with PLA/HAp composite membrane layers, which will be presented later.

3.3.3. Cytotoxicity of the membrane layers

The biosafety and biocompatibility of absorbable biomaterials should be considered since all of the treated magnesium alloy will enter into the human body. The morphology of MC3T3 cells cultured in different extraction periods for the negative control, LPM1, and LPM3 samples are presented in Fig. 10(a)–(f). Results of MC3T3 cytotoxicity tests (MTT assay) of membrane layers on Mg alloy implants are presented in Fig. 11 (extraction assay); its relation with incubation time presents RGR. It is well known and believed that both PLA and HAp have excellent biocompatibility behavior on cell viability [36,37]. Accordingly, the coated samples show good results as the number of cells increases with time, showing high bioactivity. As can be observed from light optical microscopy images (Fig. 10a–d), the cell behavior was normal and healthy. The cell growth rate increased with incubation time, especially for the coated samples, following the same trend of the negative control sample. Subsequently, the RGR level of the LPM3 (Fig. 11) is significantly higher than that of the negative control and pristine polymer membrane (LPM1 sample). The Cytotoxicity of the coated layers is safe according to the standards of the Federation de Nature International (FDI), and ISO 10993-5:1999. Moreover, it can be concluded that the membrane containing high HAp nanoparticle content is a promising candidate in terms of supporting cell growth and viability.

3.4. Mechanical properties

Biomaterials, such as bone plates and stents, are being used to substitute for human tissue, and should match the mechanical properties of tissue. The major issue is the prognosis of the evolution of degradation rate, especially in *in-vivo* tests, since the mechanical stability and degradation have to be controlled so that material will not fail during the healing process [33]. Bending strength of the coated and control samples after *in-vitro* degradation are shown in Fig. 12(a). The behavior of stress–displacement curves for the samples after 5 and 15 days immersion are shown in Fig. 12(b) and (c), respectively. It is interesting to observe that the bending strength of the uncoated samples deteriorated relatively sharply after five days (15%) of immersion tests and decreased finally by 25% after 15 days. This is due to a localized corrosion environment which creates pits around the cathodic phase and can lead to removal of nobler particles, and formation of craters, causing rapid deterioration in the mechanical properties. In contrast, the coated samples (LPM1 and LPM3) can stand long immersions, as the rate of deterioration is almost linear over time. Interestingly, the sample coated by HAp-doped PLA thin film (LPM3 sample) reveals lower decrease (4% and 10% after 5 and 15 days, respectively). Moreover, the bending strength of LPM1 at the initial period (5 days) had a relatively wide gap compared with LPM3. On the other hand, LPM1 was similar to LPM3 after 10 days. This may be related to the pH trend variation for both LPM1 and LPM3. Overall, the deposited layer can reduce the loss of mechanical integrity of the implant throughout the healing process. Therefore, we can conclude that the coating layer works as a barrier to inhibit the macro galvanic corrosion phenomenon, which supports using Mg alloys as an implant material.

4. Conclusions

Significantly, improved performance for the high corrosion rate of Mg alloys upon use as implant materials can be achieved via coating by a porous film of biodegradable polymer. Specifically, PLA is strongly recommended. Moreover, the bioactivity and the corrosion of the Mg

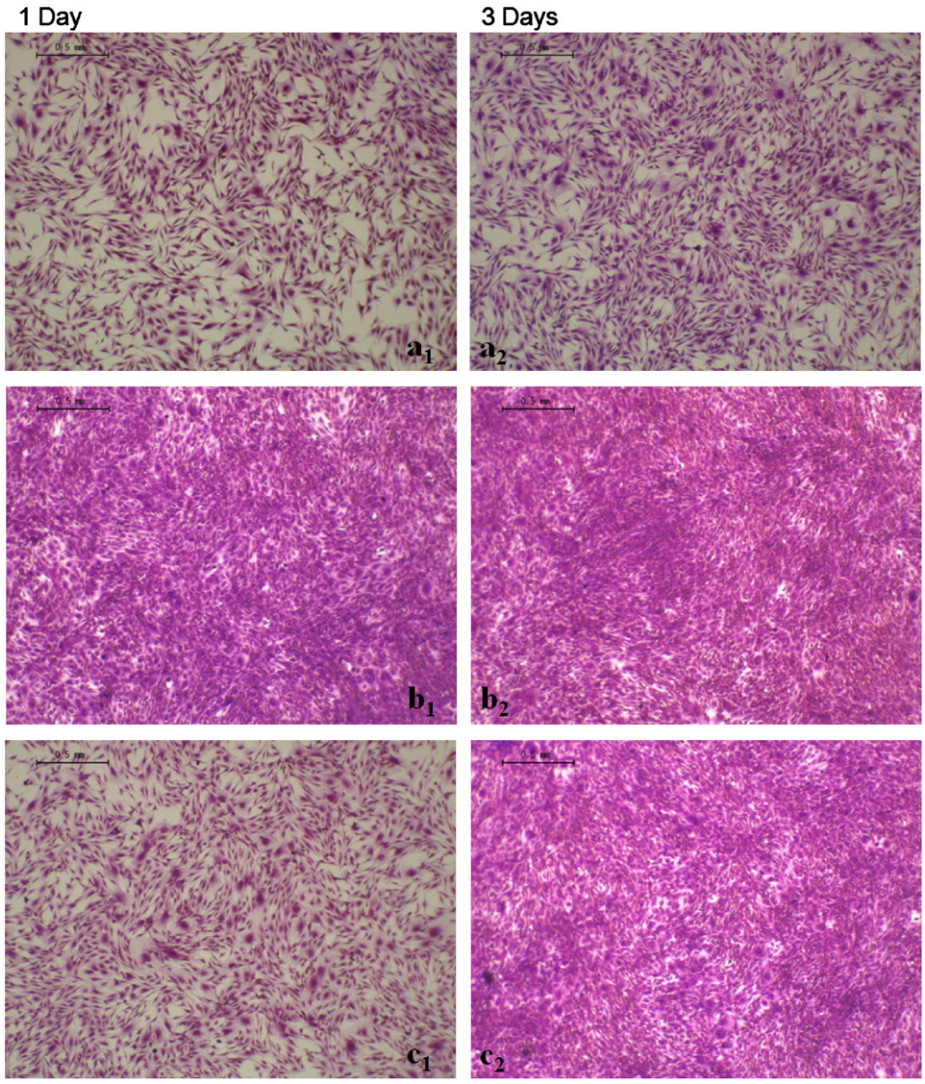

Fig. 10. MC3T3 cell morphology after 1 and 3 days incubation: (a1) and (a2) LPM1; (b1) and (b2) LPM3; (c1) and (c2) negative control (1 and 2 refer to 1 and 3 days, respectively).

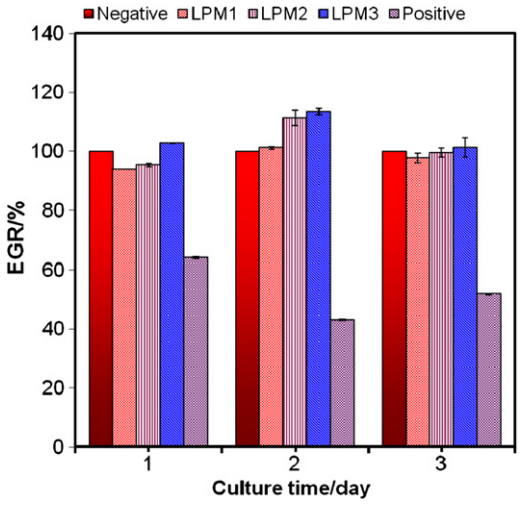

Fig. 11. Cytotoxicity testing of the membrane layers on Mg alloy implants (extraction test) on MC3T3 cell.

alloys can be distinctly improved by coating the surface by HAp-doped PLA thin film. Incorporation of HAp NPs does not affect the porosity of the thin film upon coating by the air spraying technique. Furthermore, HAp NPs accelerate the precipitation of the apatite-like materials when soaking the coated samples in the simulated body fluids, as the NPs act as nuclei for the biological apatite. Consequently, the proposed coating strategy decreases the corrosion rate of the Mg alloys as the precipitated apatite acts as barrier to isolate the metallic surface. Additionally, the coated samples seem to be harmless for MC3T3 cell growth. Furthermore, the mechanical properties of the coated samples are satisfactory. Accordingly, coating the Mg alloys with the proposed HAp-doped PLA porous thin film is a promising strategy to obtain biologically active and safe implants with acceptable corrosion rates which allow sufficient time for healing and promote cell attachment, cell growth, and cell proliferation.

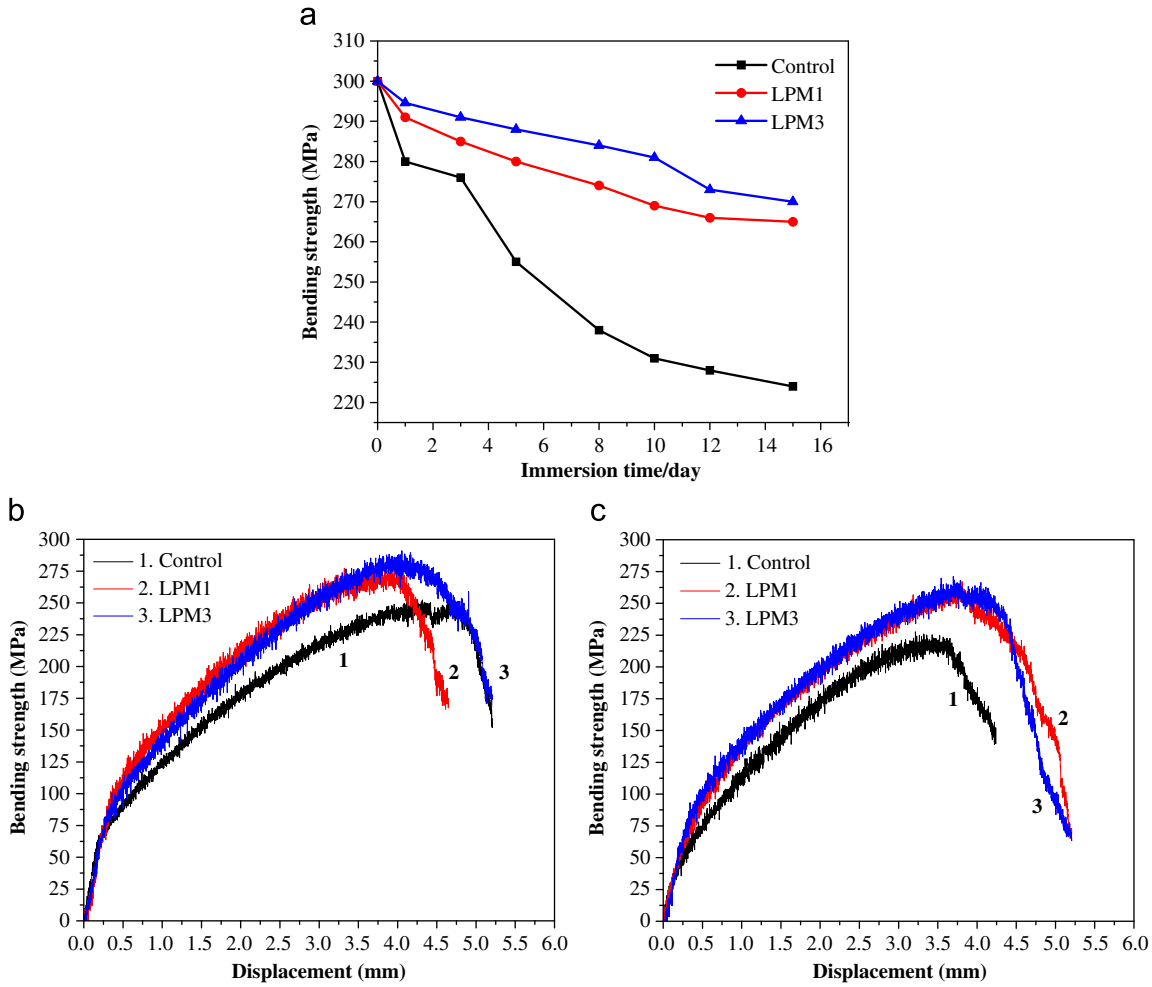

Fig. 12. Bending strength of coated and control samples during *in vitro* degradation; (a) bending strength as a correlation with the immersion time, (b) and (c) stress–displacement curves at 5 and 15 days, respectively.

Acknowledgments

This research was supported by the research funds of Chonbuk National University in 2010. In addition, the Ministry of Education, Science Technology (MEST) and the National Research Foundation of Korea (NRF) through the Human Resource Training Project, as well as Eco-friendly manufacturing technology and automation for mulberry pulp and yarns have financially supported it for Regional Innovation. The authors gratefully thank Min Ho Lee, Biomaterials and Institute of Oral Bioscience, School of Dentistry, for the donation of magnesium alloy samples; and C.W. Park, School of Mechanical Design Engineering, Chonbuk National University, for air-spray gun as a kind gift.

References

[1] M.P. Staiger, A.M. Pietak, J. Huadmai, G. Dias, Magnesium and its alloys as orthopedic biomaterials: A review, Biomaterials 27 (9) (2006) 1728–1734.

[2] M. Niinomi, Recent metallic materials for biomedical applications, Metallurgical and Materials Transactions A 33 (3) (2002) 477–486.

[3] J. Nagels, M. Stokdijk, P.M. Rozing, Stress shielding and bone resorption in shoulder arthroplasty, Journal of Shoulder and Elbow Surgery 12 (1) (2003) 35–39.

[4] J.E. Gray-Munro, C. Seguin, M. Strong, Influence of surface modification on the in vitro corrosion rate of magnesium alloy AZ31, Journal of Biomedical Materials Research Part A 91A (1) (2009) 221–230.

[5] B. Denkena, F. Witte, C. Podolsky, A. Lucas, Degradable implants made of magnesium alloys, in: Proceedings of 5th Euspen International Conference-Montpellier, France, 2005.

[6] E.D. McBride, Magnesium screw and nail transfixation in fractures, Southern Medical Journal 31 (1938) 508–515.

[7] B. Zberg, P.J Uggowitzer, J.F. Löffler, MgZnCa glasses without clinically observable hydrogen evolution for biodegradable implants, Nature Materials 8 (2009) 287–291.

[8] Z. Li, X. Gu, S. Lou, Y. Zheng, The development of binary Mg–Ca alloys for use as biodegradable materials within bone, Biomaterials 29 (10) (2008) 1329–1344.

[9] X. Gu, Y. Zheng, S. Zhong, J.W. Tingfei Xi, W. Wang, Corrosion of, and cellular responses to Mg–Zn–Ca bulk metallic glasses, Biomaterials 31 (2010) 1093–1103.

[10] G. Wang, H. Zreiqat, Functional coatings or films for hard-tissue, Applications Materials 3 (2010) 3994–4050.

[11] F. Witte, J. Fischer, J. Nellesen, H.-A. Crostackb, A.P. Volker Kaesec, F. Beckmann, H. Windhagen, In vitro and in vivo corrosion measurements of magnesium alloys, Biomaterials 27 (2006) 1013–1018.

[12] H.M. Wong, K.W.K. Yeung, V.T. Kin On Lam, K.D.K.L. Paul K. Chu, K.M.C. Cheung, A biodegradable polymer-based coating to control the performance of magnesium alloy orthopaedic implants, Biomaterials 31 (2010) 2084–2096.
[13] N.A.M. Barakat, F.A. Sheikh, S.S. Al-Deyab, I.S. Chronakis, H.Y. Kim, Biologically active polycaprolactone/titanium hybrid electrospun nanofibers for hard tissue engineering, Science Advanced Materials 3 (5) (2011) 730–734.
[14] K.A. Khalil, S.W. Kim, N. Dharmaraj, K.W. Kim, H.Y. Kim, Novel mechanism to improve toughness of the hydroxyapatite bioceramics using high-frequency induction heat sintering, Journal of Materials Processing Technology (2007) 417–420.
[15] N.A.M. Barakat, K.A. Khalil, F.A. Sheikh, A.M. Omran, B. Gaihre, S.M. Khil, H.Y. Kim, Physiochemical characterizations of hydroxyapatite extracted from bovine bones by three different methods: Extraction of biologically desirable HAp, Materials Science and Engineering: C 28 (8) (2008) 1381–1387.
[16] D.-Y. Lin, X.-X. Wang, Preparation of hydroxyapatite coating on smooth implant surface by electrodeposition, Ceramics International 37 (1) (2011) 403–406.
[17] J. Szymura-Oleksiak, A. Ślósarczyk, A. Cios, B. Mycek, Z. Paszkiewicz, S. Szklarczyk, D. Stankiewicz, The kinetics of pentoxifylline release in vivo from drug-loaded hydroxyapatite implants, Ceramics International 27 (7) (2001) 767–772.
[18] B. Chen, T. Zhang, J. Zhang, Q. Lin, D. Jiang, Microstructure and mechanical properties of hydroxyapatite obtained by gel-casting process, Ceramics International 34 (2) (2008) 359–364.
[19] F. Witte, F. Feyerabend, P. Maier, J. Fischer, M. Störmer, C. Blawert, W. Dietzel, N. Hort, Biodegradable magnesium hydroxyapatite metal matrix composites, Biomaterials 28 (13) (2007) 2163–2174.
[20] A. International, ASTM G102 - Standard Practice for Calculation of Corrosion Rates and Related Information from Electrochemical Measurements, in, Vol. 89, US, (Reapproved 2010), p. 7.
[21] B. Nasiri-Tabrizi, P. Honarmandi, R. Ebrahimi-Kahrizsangi, P. Honarmandi, Synthesis of nanosize single-crystal hydroxyapatite via mechanochemical method, Materials Letters 63 (2009) 543–546.
[22] S. Nayar, M.K. Sinha, D. Basu, A. Sinha, Synthesis and sintering of biomimetic hydroxyapatite nanoparticles for biomedical applications, Journal of Materials Science: Materials in Medicine 17 (2006) 1063–1068.
[23] Y. Sun, G. Guo, Z. Wang, H. Guo, Synthesis of single-crystal HAp nanorods, Ceramics International 32 (8) (2006) 951–954.
[24] G. Guo, Y. Sun, Z. Wang, H. Guo, Preparation of hydroxyapatite nanoparticles by reverse microemulsion, Ceramics International 31 (6) (2005) 869–872.
[25] G. Bierwagen, The physical chemistry of organic coatings revisited-viewing coatings as a materials scientist, Journal of Coatings Technology and Research 5 (2) (2008) 133–155.
[26] G. Grundmeier, W. Schmidt, M. Stratmann, Corrosion protection by organic coatings: electrochemical mechanism and novel methods of investigation, Electrochimica Acta 45 (15–16) (2000) 2515–2533.
[27] P.A. Sørensen, S. Kiil, K. Dam-Johansen, C.E. Weinell, Anticorrosive coatings: a review, Journal of Coatings Technology and Research 6 (2) (2009) 135–176.
[28] H.-C. Liu, I.-C. Lee, J.-H. Wang, S.-H. Yang, T.-H. Young, Preparation of PLLA membranes with different morphologies for culture of MG-63 Cells, Biomaterials 25 (18) (2004) 4047–4056.
[29] J. Zheng, A. He, J. Li, J. Xu, C.C. Han, Studies on the controlled morphology and wettability of polystyrene surfaces by electrospinning or electrospraying, Polymer 47 (24) (2006) 7095–7102.
[30] L. Jin-Bo, L. Xuan-Yong, L. Wei-Feng, Z. Jian-Hao, Preparation and characterization of bioactive poly (lactic acid)/SiO2-CaO composite membranes, Inorganic Materials 26 (9) (2011) 998–1002.
[31] A.F.S. Zereshki, S.S. Madaeni, S. Simonec, J.C. Jansenc, M. Esmailinezhada, E. Drioli, Poly(lactic acid)/poly(vinyl pyrrolidone) blend membranes: Effect of membrane composition on pervaporation separation of ethanol/cyclohexane mixture, Membrane Science 362 (2010) 105–112.
[32] V. von MSc-Chemiker, T.F.d. Conceição, A. Brasilien, Corrosion protection of magnesium AZ31 alloy sheets by polymer coatings, in: GKSS Materials Vol. PhD, Research Center, Max-Plank Strasse Geesthacht, Germany, 2011, p. 171.
[33] W.-D. Mueller, M.L. Nascimento, M.F.L.d. Mele, Critical discussion of the results from different corrosion studies of Mg and Mg alloys for biomaterial applications, Acta Biomaterialia 6 (5) (2010) 1749–1755.
[34] H. Zhou, J. Lee, Nanoscale hydroxyapatite particles for bone tissue engineering, Acta Biomaterialia 7 (7) (2011) 2769–2781.
[35] C. Di Mario, H. Griffiths, O. Goktekin, N. Peeters, J. Verbist, M. Bosiers, K. Deloose, B. Heublein, R. Rohde, V. Kasese, C. Ilsley, R. Erbel, Drug-eluting bioabsorbable magnesium stent, Journal of Interventional Cardiology 17 (6) (2004) 391–395.
[36] H.K. Varma, S. Suresh Babu, Synthesis of calcium phosphate bioceramics by citrate gel pyrolysis method, Ceramics International 31 (1) (2005) 109–114.
[37] S. Ramesh, C.Y. Tan, W.H. Yeo, R. Tolouei, M. Amiriyan, I. Sopyan, W.D. Teng, Effects of bismuth oxide on the sinterability of hydroxyapatite, Ceramics International 37 (2) (2011) 599–606.